ACS OMEGA

http://pubs.acs.org/journal/acsodf

Article

# Carbon Nano-Onion-Decorated ZnO Composite-Based Enzyme-Less Electrochemical Biosensing Approach for Glucose

Ankita Sharma, Ankush Agrawal, Gaurav Pandey, Sanjay Kumar, Kamlendra Awasthi,* and Anjali Awasthi*

Cite This: *ACS Omega* 2022, 7, 37748−37756

Read Online

ACCESS | Metrics & More | Article Recommendations

**ABSTRACT:** This study investigates the enzyme-less biosensing property of the zinc oxide/carbon nano-onion (ZnO/CNO) nanocomposite coated on a glassy carbon electrode. The ZnO/CNO nanocomposite was synthesized using the ex situ mixing method, and the structural characterization was done using XRD, SEM, and TEM, whereas functional groups and optical characterization were done through FTIR and UV−visible spectroscopy. The electrochemical sensing response of the ZnO/CNO nanocomposite for the linear range of glucose concentration (0.1−15 mM) was examined using cyclic voltammetry (CV) with a potential window of −1.6 to +1.6 V using 0.1 M NaOH as an electrolyte. The ZnO/CNO nanocomposites showed enhanced sensing ability toward glucose with a sensitive value of 606.64 $\mu$A/mM cm$^2$. Amperometric i-t measurement supports the finding of CV measurement and showed good sensing ability of the electrode ZnO/CNO nanocomposite material for up to 40 days. The enhanced electrocatalytic activity of the ZnO/CNO nanocomposite is explained due to the synergetic effect of both ZnO and CNO. Our findings suggest a high potential for ZnO/CNO nanocomposite-based glucose biosensors, which could be further utilized to develop noninvasive skin-attached sensors for biomedical applications.

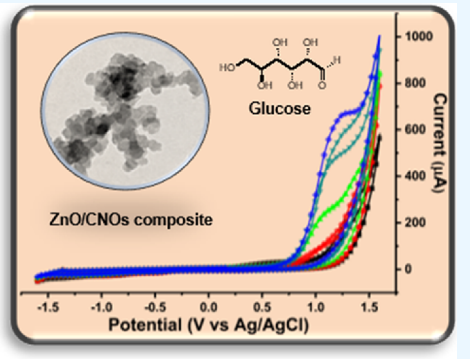


## 1. INTRODUCTION

Glucose level determination is critical in clinical diagnostics along with environmental and ecological fields, food and microbiology industries, wastewater treatment, and so on.[1,2] The International Diabetes Federation (IDF) predicts that by 2045, there would be 783 million people worldwide with diabetes, which is one of the fastest-growing global health emergencies.[3] Hence, it has become crucial to employ suitable treatment to examine and measure the level of glucose in the human blood. As a result, glucose biosensors have emerged as the most active area of sensor development. The initial biosensors investigated in the field of glucose analysis were enzymatic and nonenzymatic glucose sensors based on widely used techniques such as optical, acoustic, electrochemical, and fluorescence. Enzymatic electrochemical biosensors[4,5] are often used as glucose biosensors, but because of changes in pH, humidity, and temperature, their sensitivity changes. Also, they are highly unstable and expensive and require sophisticated immobilization techniques.[6,7] Therefore, significant efforts have been made in the direction of the fabrication of enzyme-less biosensors that are affordable, sensitive, rapid, and dependable.[8−10] Nonenzymatic biosensors have been designed with the application of nanomaterials like carbonaceous structures, metal and metal-oxide nanostructures, hydrogels, and conductive polymeric substances. The increased relative surface area and the quantum effects are the two main reasons for a significant difference in the characteristics of nanomaterials, leading these to act as a nano-catalyst.[11] Properties including reactivity, strength, and electrical conductivity can be altered or improved as a result of these considerations.[12−14]

Metal-oxide-based nanostructures have been in the last decade as enzyme-less glucose biosensors due to their improved sensing efficiency, which includes sensitivity, response time, and accuracy. These nanomaterials provide large specific surfaces and particular physical features that boost the catalytic power. The biosensor's performance is known to be influenced by the interface generated when nanostructured metal oxide (NMO) binds to a biomolecule.[15] Biomolecules connect to metal-oxide nanoparticles in a variety of ways, including physical adsorption and chemical binding.[16,17]

**Received:** July 27, 2022
**Accepted:** September 27, 2022
**Published:** October 11, 2022

Nonenzymatic metal-oxide-based electrochemical biosensors are now mostly based on semiconductor materials like zinc oxide (ZnO),[18] cuprous oxide ($Cu_2O$),[19] tin oxide ($SnO_2$),[20] and others. ZnO has piqued the interest of many scientists among metal oxides for two key reasons; i.e., first, zinc oxide is a popular n-type II−IV semiconductor having a band gap of roughly 3.37 eV with desirable attributes such as chemical stability, adaptability of doping, non-toxicity, and high optical properties,[21] and second, a vast variety of morphologies can be attained with derivatives. The biosensing characteristics of ZnO nanostructures are greatly influenced by the size, morphology, and crystallinity of synthesized ones. Even today, ZnO is the preferred nanomaterial for biosensing purposes among researchers.[22] It is widely applied for different sensing techniques such as electrochemical sensing[23,24] and optical sensing.[25,26] Along with the biosensing applications, ZnO has been widely applied for gas sensing purposes as well due to its fast response, low manufacturing cost, and high selectivity.[27,28] Several strategies have been reported for determining glucose through ZnO where recently nine ZnO nanostructures were synthesized using multi-walled carbon nanotubes (MWCNTs) assisted with amino acids, and in this enzyme-less biosensor system, spherical ZnO formulated from zinc acetate/cysteine/oxalic acid exhibits a maximum sensitivity of 64.29 $\mu A/cm^2$ mM with consistent findings.[29] Similarly, an iron-doped ZnO nanoparticle-based screen-printed working electrode was fabricated for sensing glucose, which achieved a low limit of detection, i.e., 0.30 $\mu$m,[30] whereas a copper-doped ZnO-based impedimetric glucose sensor exhibited a large linear range from $10^{-9}$ to $10^{-5}$ M.[31]

Carbon nanomaterials such as fullerenes, carbon nanotubes, graphene oxide (GO), carbon quantum dots, carbon black, nano-diamonds, and carbon nano-onions (CNOs) have intrinsic properties that can be effortlessly applied in the development of advanced technology for sensing applications.[32−35] Drawbacks related to other carbon structures such as CNTs and GO include the typical procedure for their synthesis, higher toxicity of GO, and the lesser aqueous solubility of CNTs, which can be overcome in the case of CNOs. Nowadays, CNOs are preferred over other carbon nanostructures due to their unique combination of properties such as conductivity, thermal stability, biocompatibility, non-toxicity, and the feasibility during the formation of composites with functional groups or coupling with organic or inorganic polymers. Such traits made them a promising candidate for several applications like energy storage, biomedical applications, bioimaging, and sensing. Therefore, with such excellent properties, CNOs and their composites are now in demand for biosensing applications for glucose, and an increasing trend has been observed due to satisfactory results.[36−38] In recent work, Pt nanoparticles (2.5 nm) coated on CNOs have been found to exhibit glucose detection within the range of 2−28 mM, and the observed limit of detection (LOD) was 0.09 mM.[39] The photoluminescence sensor was designed by using water-soluble CNOs for selective determination of glucose which was based on the turn-off and turn-on technique,[40] whereas in another study, Pd-doped CNOs were used for the glucose oxidation reaction in the range between 5 and 8 mM.[41] The purpose of choosing the ZnO/CNO composite is to utilize their advances synergistically for sensing purposes, and both ZnO and CNOs were reported singly for glucose sensing, but their composite has not been explored yet.

Here, in this report, the ZnO/CNO nanocomposite was investigated to study glucose detection, and our work is depicted through the schematic shown in Figure 1. A simple

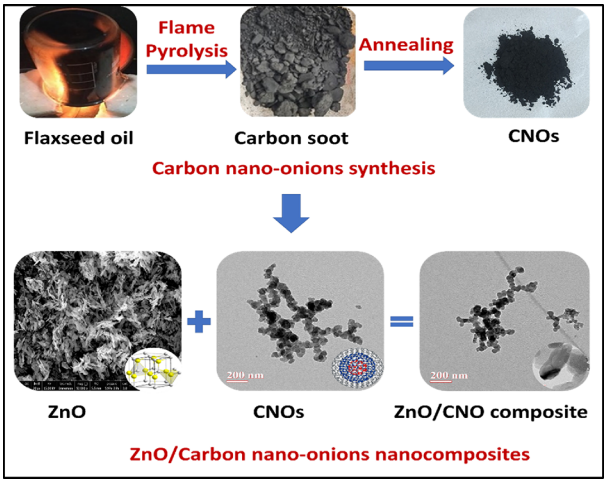


**Figure 1.** Schematic representation of the ZnO/CNO nanocomposite for glucose biosensing.

procedure was used to create a hybrid CNO-functionalized ZnO composite. Mixing through ultrasonication to modify the surface of chemically synthesized ZnO peanut-shaped rods with CNOs was done. The CNOs have been synthesized using flaxseed oil as a precursor. Along with high potential properties for sensing, CNOs have also been chosen over other carbon nanostructures due to their easy synthesis method, long-term stability, and cost-effectiveness. It was expected that high electron transfer rates of ZnO combined with the robust catalytic reaction of CNOs will provide an excellent platform for glucose sensing, and the results met our expectations. So far, both the nanomaterials are applied for the determination of glucose either singly or with others as nanocomposites, but their combination has not been reported yet. The ZnO and CNO cyclic voltammetry (CV) results have also been recorded for comparative analysis. A remarkable improvement in the overall determination was analyzed with the ZnO/CNO composite rather than these nanostructures alone.

## 2. RESULTS AND DISCUSSION

ZnO is one of the popular nanomaterials in biosensing technologies due to its advantageous properties and traits such as a wide range of morphologies, optical and electrochemical properties, biocompatibility, and stability allow it to be a perfect candidate for designing nonenzymatic electrochemical biosensors.[42−45] Apart from this, CNOs have also diverged the attention of researchers due to their efficient properties and cost-effectiveness in biosensing applications.[46]

**2.1. Characterization of ZnO, CNO, and ZnO/CNO Composites.** ZnO nanostructures have been successfully synthesized by the method described in the Experimental Section. SEM images of the prepared ZnO are shown in Figure 2a, and it is observed that ZnO nanostructures obtained the shape of rods broadened at the ends resembling peanut-shaped rods. The length of the nanostructures is approximately 0.2−0.4 microns in size. However, when compared to XRD, the range of view and detection depth of SEM are limited, and the size acquired by XRD should be lesser than that obtained by SEM. Carbon onions are separately prepared and annealed


https://doi.org/10.1021/acsomega.2c04730
ACS Omega 2022, 7, 37748−37756

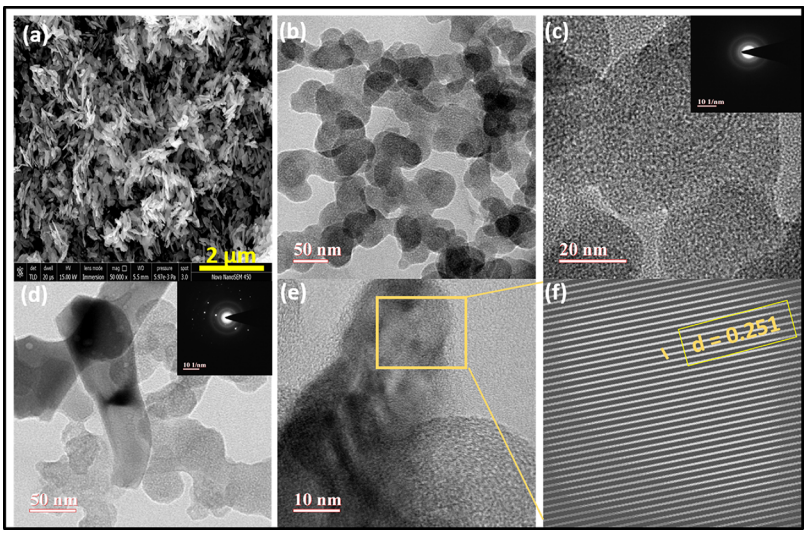


**Figure 2.** (a) SEM images of ZnO nanostructures. (b) TEM image of CNOs at a 50 nm scale range. (c) TEM image of CNOs with high resolution at a 20 nm scale range, and the inset shows the SAED pattern of the same. (d) TEM image of the ZnO/CNO nanocomposite depicting large rods as ZnO structures and CNOs as spherical rings, and the inset shows the SAED pattern of the prepared composite. (e) HRTEM image of the ZnO/CNO composite. (f) The interplanar spacing of ZnO in the ZnO/CNO composite.

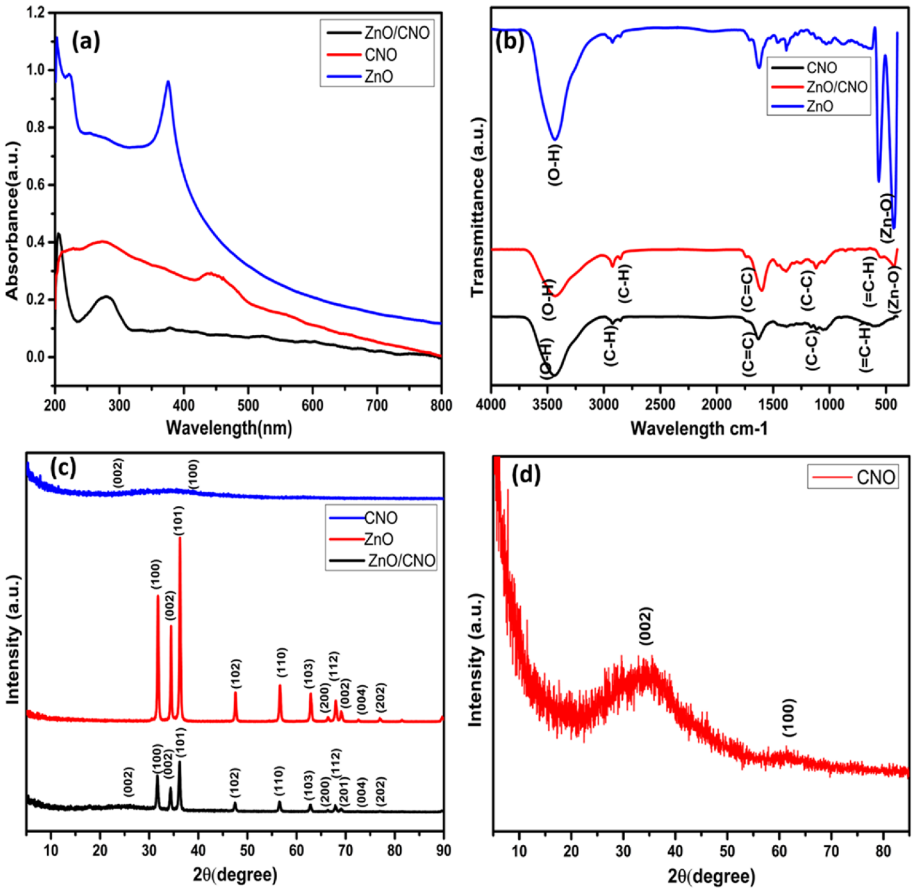


**Figure 3.** (a) UV−vis spectra of ZnO, CNO, and ZnO/CNO in the range of 200−800 nm. (b) FTIR spectra of ZnO, CNO, and ZnO/CNO in the range of 400−4000 $cm^{-1}$ wavelength. (c) XRD pattern of CNO, ZnO, and ZnO/CNO (comparative). (d) CNO XRD pattern representing characteristic peaks.

through the described methodology. High-resolution transmission electron microscopy (HRTEM) images of CNOs and ZnO/CNO composite give better detailing of their structures compared to SEM analysis. CNOs resemble fullerenes that are spherically closed carbon shells and possess concentric fullerenes wrapped one inside the other, thus forming an onion-like structure. The surface morphology of CNOs was elucidated by TEM images depicted in Figure 2b. The average size of the synthesized CNOs is found to be 40−50 nm, whereas in Figure 2c, the inset represents the selected area



https://doi.org/10.1021/acsomega.2c04730
ACS Omega 2022, 7, 37748−37756

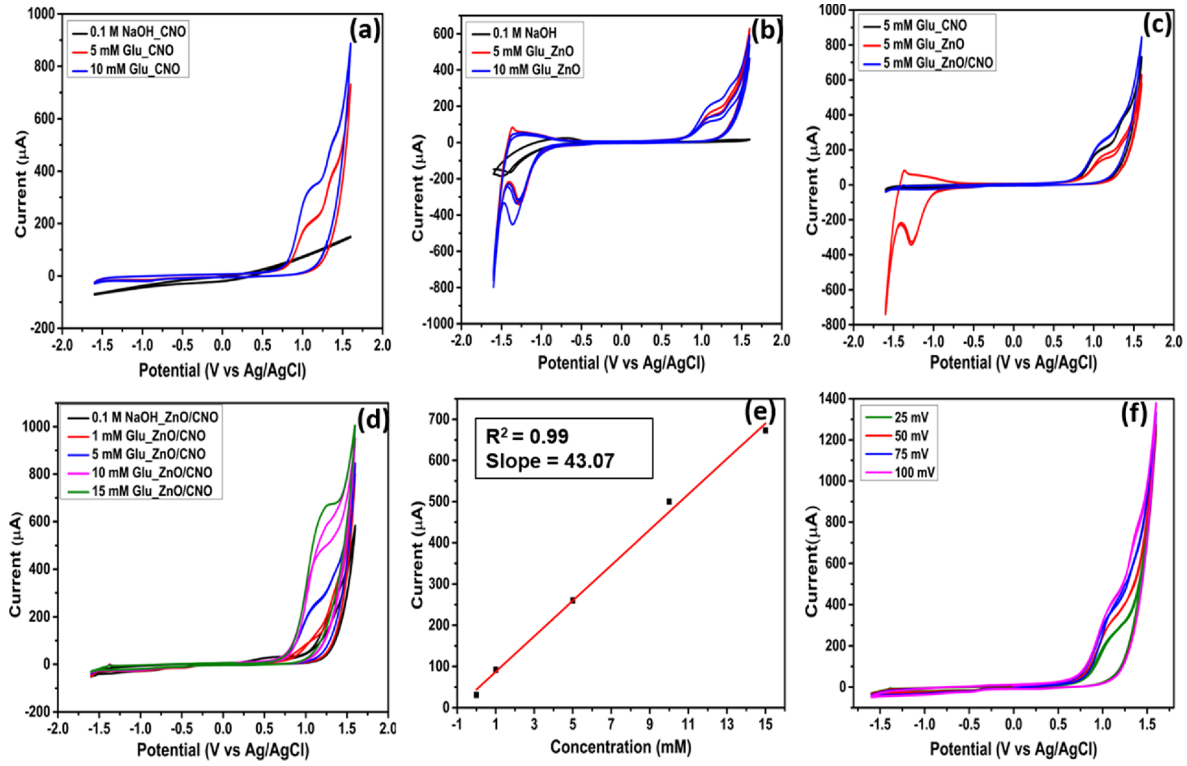


**Figure 4.** (a) CV curves of the CNO GC electrode without glucose and with glucose (5 and 10 mM) in 0.1 M NaOH electrolyte solution at a 50 mV scan rate. (b) CV curves of the ZnO GC electrode without glucose and with glucose (5 and 10 mM) in 0.1 M NaOH electrolyte solution at a 50 mV scan rate. (c) Comparative curves of CNO, ZnO, and ZnO/CNO GC electrodes with a 5 mM glucose concentration in 0.1 M NaOH at a 50 mV scan rate. (d) CV curves for the ZnO/CNO GC electrode for different concentrations of glucose (1−15 mM) at a scan rate of 50 mV/s. (e) Linear calibration curve of ZnO/CNO for different concentrations of glucose. (f) CV curves for ZnO/CNO with 5 mM concentration of glucose at different scan rates.

electron diffraction (SAED) pattern of CNOs. The SAED pattern is performed using transmission electron microscopy and is used to detect crystal orientation, quantify lattice constants, and investigate flaws, particularly when combined with proper analytical tools. The SAED pattern of CNOs demonstrates the existence of graphitic carbon and diamond-like carbon that is verified by the XRD results as well and seems interconnected in a chained network. ZnO/CNO composite morphological detailing was also executed through TEM analysis and can be observed in Figure 2d,e where it can be seen that CNOs are dispersed onto the surface of the ZnO rods and the average size was around 300 nm. The HRTEM images also verified the hexagonal wurtzite structure of ZnO, showing clear lattice fringes with an interplanar spacing of 0.25 nm, which corresponds to the (101) plane of the ZnO hexagonal phase shown in Figure 2f.

Apart from the morphology and structural details, other properties such as the crystal structure and phase, optical properties, and chemical composition of the synthesized nanostructures are revealed through XRD patterns, UV−vis absorption, and FTIR characterizations.

UV−vis spectroscopy was used to determine the optical properties of our synthesized nanomaterials, and these properties are used to determine other parameters as well such as photocatalytic activity. The excitation peak of the UV−vis absorption spectra of ZnO peanut-shaped rods and ZnO/CNO are observed at 375 nm and 280 nm, respectively, which is illustrated in Figure 3a, and these were due to electrons directly transitioning between the valence and the conduction bands.

The major absorption peaks of ZnO and CNOs could be observed in the UV−vis spectra. By extrapolating the linear section of the graph between the function $(h\upsilon)^2$ versus photon energy $(h)$, the band gap energy of ZnO, CNO, and ZnO/CNO composite nanostructures could be estimated, which is found to be 3.09, 2.34, and 3.52 eV, respectively. This band gap shift might be related to electron constraints, which have been reported in a variety of nanomaterials, and also due to their differences in morphological structures, defects, and grain size confinement.[47]

Fourier transform infrared spectroscopy generates the sample's molecular fingerprint as the resultant signal because various chemical structures yield distinct spectral signatures, thus helping in determining the chemical composition of these prepared nanomaterials. The FTIR spectra of ZnO, ZnO/CNO, and CNOs are depicted in Figure 3b. The ZnO FTIR spectrum exhibits a characteristic peak representing O−H stretching vibrations at 3434 $cm^{-1}$ and a strong peak owing to Zn−O vibrations at 433 $cm^{-1}$. The graphitic carbon peaks are observed in the FTIR spectrum of CNOs. Alkyl C−H stretching, C═C stretching, C−C stretching, and ═CH bending vibrations are ascribed to the doublet at 2922 $cm^{-1}$, a strong peak at 1630 $cm^{-1}$, a medium band at 1059 $cm^{-1}$, and a broadband at 591 $cm^{-1}$, respectively. Surface O−H moiety and chemisorbed water are accountable for the wide peak at 3437 $cm^{-1}$. Most of the distinctive peaks of the CNOs and ZnO are evident in the ZnO/CNO composite with minor alterations in peak positions due to strong chemical and physical interactions between CNO and ZnO, which are as follows: 3432 $cm^{-1}$ (O−H wide band), 2923 $cm^{-1}$ (−CH doublet), 1600 $cm^{-1}$ (C═C


https://doi.org/10.1021/acsomega.2c04730
ACS Omega 2022, 7, 37748−37756

strong), 1045 $cm^{-1}$ (C−C stretching), 542 $cm^{-1}$ (=CH banding), and 431 $cm^{-1}$ (Zn−O stretching vibrations).[48]

The crystallinity and crystal phase were studied by X-ray diffraction. Figure 3c illustrates the XRD patterns of the CNO, ZnO, and ZnO/CNO composites. The hexagonal wurtzite crystal structure of ZnO peanut-shaped rods is depicted through XRD patterns and analyzed by X'Pert HighScore Plus software with standard JCPS card no. 01-079-0205. Our synthesized ZnO nanostructures match 96% with the standard reference structure, and characteristic sharp peaks represent the hexagonal crystal structure, and the average crystallite size obtained is 27.83 nm. The characteristic diffraction peaks of ZnO are assigned to planes (100), (002), (101), (102), (110), (103), (200), (112), (201), (004), and (202) according to JCPS card no. 01-079-0205. The purity of the prepared ZnO could be attributed to no other peaks. The XRD pattern of CNOs in Figure 3d illustrates two diffraction peaks at $2\theta$ at near 35 and 60 corresponding to (002) and (100) planes representing the crystalline nature of CNOs in a hexagonal graphitic carbon form. Both the characteristic diffraction peaks of ZnO and CNO are observed in the XRD pattern of the ZnO/CNO composite.

**2.2. Enzyme-Less Glucose Behavior of ZnO, CNO, and ZnO/CNO Fabricated Electrodes.** The cyclic voltammograms of CNO, ZnO, and ZnO/CNO electrodes in 0.1 M NaOH are represented in Figure 4. In the absence of glucose, no oxidation peaks were observed for the bare ZnO, CNO, and ZnO/CNO. Before testing the ZnO/CNO composite, separate cyclic voltammograms have been recorded for ZnO and CNO electrodes to check their sensitivity toward glucose, as shown in Figure 4a,b. When a small amount of glucose (5 mM) is added to the solution, prominent oxidation peaks were observed at 1.10, 1.10, and 1.11 V for CNO, ZnO, and ZnO/CNO, respectively. These well-defined oxidation peaks at 1.1 V correspond to the electro-oxidation of glucose at the surface of the electrode.[49] This also confirms the strong sensing ability property of CNO and ZnO toward glucose. Enhancement in the peak current value with the addition of more glucose represents an increase in sensing ability. For 5 mM concentration of glucose, the peak current value of ZnO/CNO is found to be highest (285 $\mu$A) compared with the bare CNO (220 $\mu$A) and bare ZnO (180 $\mu$A), as depicted in Figure 4c, which confirms the higher sensing ability of ZnO/CNO compared with the pristine one. The current peak intensities increased with increasing concentration from 1 to 15 mM glucose for ZnO/CNO, which is depicted in Figure 4d. The higher the current peak intensities, the higher will be the sensitivity, as these are directly proportional to each other. Figure 4f illustrates the CV curves recorded at different scan rates at a single concentration, i.e., 5 mM glucose showing the current increment with the rise in the potential scan rate. There were no oxidation peaks observed with bare GCE and in the absence of glucose, but sharp peaks in the presence of glucose determined the specific detection of the target analyte through fabricated electrodes. The enhanced sensing property of ZnO/CNO can be attributed to the enhancement in the conductivity of ZnO. Overall, ZnO-based electrochemical sensing of glucose can be expressed as

$$\text{glucose} + O_2 + H_2O = \text{gluconic acid} + H_2O_2$$

$$Zn^{+2}(OH)^-_2 + OH^- = Zn^{+2}O^-(OH)^- + H_2O + e^-$$

$$Zn^+(OH)^- + \text{glucose} = Zn^{+2}(OH)^-_2 + \text{gluconic acid}$$

Figure 4e depicts the calibration curve, which is plotted by averaging currents across a wide range of potentials. At a smaller-scale concentration range, the calibration data matched well linearly, allowing the slope to be estimated. Finally, using the equation below, the acquired slope value was divided by the value of the electrode's active surface area.

$$\text{sensitivity} = \text{slope}\ (\mu A\ mM^{-1})/\text{area}\ (cm^2)$$

The electrode sensitivity of ZnO/CNO is calculated to be 606.64 $\mu$A $mM^{-1}$ $cm^{-2}$, which is much better than the previously reported nonenzymatic-based sensors. The determination coefficient was found to be 0.995. Here, the minimum concentration used for glucose determination with ZnO/CNO GCE was 0.1 mM, and the results show significant sensitivity. The higher value of sensitivity of ZnO/CNO is due to the synergetic effect of both CNO and ZnO, as the modified ZnO/CNO electrode accelerates the electrochemical reaction of glucose.

The comparative results of our work and previously reported nonenzymatic-based glucose sensors are summarized in Table 1.

**Table 1. Analytical Performance of Nonenzymatic Electrochemical Sensors for Detection of Glucose**

| S.N. | nanomaterial | sensitivity ($\mu A\ mM^{-1}\ cm^{-2}$) | linear range | reference |
|---|---|---|---|---|
| 1 | ZnO/CNO | 606.64 | 0.1−15 mM | this work |
| 2 | MWCNT/ZnO QDs | 9.36 | 0.1−2.5 $\mu$M | 18 |
| 3 | SWCNTs/$Cu_2O$/ZnO NRs | 289.8 | 11.11 mM | 50 |
| 4 | SWCNTs/$Cu_2O$/ZnO NRs/graphene | 466.1 | 0.6−11.1 mM | 50 |
| 5 | $Cu_2O$−ZnO | 441.2 | 0.02−1 mM | 51 |
| 6 | nano-copper oxide micro hollow spheres | 25.0 ± 0.8 | 1 $\mu$M to 3 mM; 3−11.5 mM | 19 |
| 7 | ZnO/MWCNT/GCE | 64.29 | 1−10 mM | 29 |
| 8 | $Cu_2O$/chemical-reduced graphene | 285 | 0.3−3.3 mM | 52 |

Our findings suggest that the ZnO/CNO-based nanocomposites may serve as a significant facilitator, provided a larger surface area, and improved electron transfer kinetics.

**2.3. Amperometry I-T and Interference Study-Based Sensor Performance.** Several key attributes of the biosensors have been assessed, including sensitivity, anti-interference, and repeatability. One of the sensor's primary properties is its selectivity about various interfering agents present along with the analyte of interest.[5] Biomolecules that interfere with high polarization voltage include ascorbic acid, uric acid, lactic acid, and citric acid found in body fluids, where they oxidize and provide false signals. Figure 5a shows the selectivity test for the ZnO/CNO working electrode to detect glucose with interfering species citric acid (CA), ascorbic acid (AA), lactic acid (LA), ethanol, glycerol, and urea present in 0.1 mM concentration and thus proven as highly selective toward glucose. First, 0.1 mM glucose was added to 0.1 M NaOH electrolyte solution on which the current peak rises, which does not change with the addition of 0.1 mM AA. After the



https://doi.org/10.1021/acsomega.2c04730
ACS Omega 2022, 7, 37748−37756

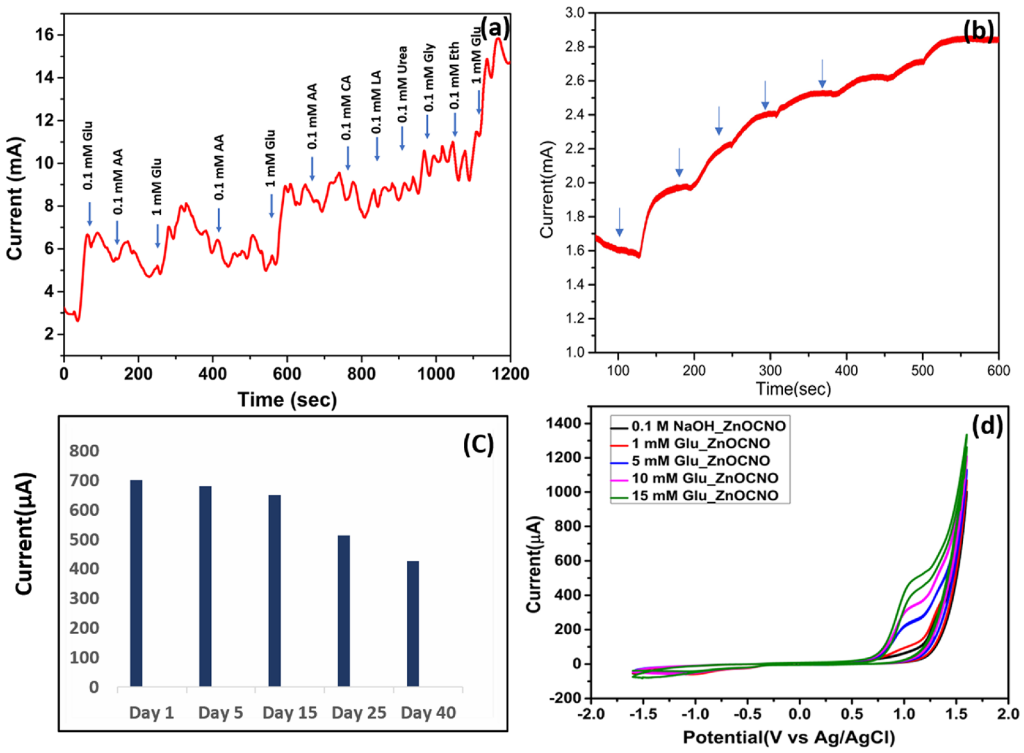


**Figure 5.** (a) Interference study plot that shows the amperometric response for glucose of the ZnO/CNO GC electrode in the presence of various interferents such as citric acid, ascorbic acid, and urea (all with a concentration of 0.1 mM) in 0.1 M NaOH electrolyte at 0.60 V with a 0.05 sample interval. (b) Amperometric plot on successive addition of 2 mM glucose in 0.1 M NaOH at 0.65 V. (c) Plot exhibiting a reduction in the current peak through repeatability studies although having the potential to sense glucose after 40 days. (d) CV studies after 40 days with the same modified working electrode with different concentrations of glucose in 0.1 M NaOH electrolyte solution.

addition of 2 mM glucose concentration, 0.1 mM concentration of interfering species was added at a constant interval during which the current intensity does not change. Lastly, when 1 mM glucose was introduced to the system, there was a sharp rise in the current signal. Investigating the influence of interfering species reveals how well the system can distinguish the target analyte molecule from the other substances present in the sample. Figure 5b shows the amperometric detection demonstrated in a stair-like response of current density to glucose concentrations. Here, upon the addition of 2 mM glucose at a fixed interval, a significant rise in the current intensity has been observed. The repeatability test was measured by testing the same modified GCE for consecutive days, and the CV results after 40 days are depicted in Figure 5d. The graph in Figure 5c shows a decrease in the current peak intensities from 700 to 430 $\mu$A after 40 days but still has the potential to sense glucose at lower concentrations. Although the stability is not that high according to the results, it could sense glucose with good sensitivity comparable to previously reported sensors. We can work out stability enhancement by changing the ratios of ZnO to CNOs in the extension of the work.

## 3. CONCLUSIONS

In this work, ZnO/CNO composite-based working electrodes were fabricated and employed for glucose level monitoring. The synthesis of ZnO/CNO followed a three-step production method that included the synthesis of ZnO and CNO followed by the decoration of ZnO nano-peanuts with CNOs. SEM and TEM images reveal the morphology and size of ZnO nanostructures (0.2−0.4 microns), CNOs (40−50 nm), and ZnO/CNO (0.3 microns). The crystallite phases, band gap energies, and chemical composition of ZnO (hexagonal wurtzite structure; 3.09 eV), CNOs (hexagonal graphite carbon; 2.34 eV), and ZnO/CNO (3.52 eV) have been confirmed through XRD data, UV−vis spectra, and FTIR spectra, respectively. The designed sensor demonstrated a high sensitivity of 606.64 $\mu$A mM$^{-1}$ cm$^{-2}$ with a linear range of 0.1−15 mM glucose concentration and a determination coefficient of 0.995. This sensor has anti-interference properties and long-term stability. Sensitivity toward glucose remains unaffected by the presence of interfering species named citric acid, urea, lactic acid, glycerol, ethanol, and ascorbic acid. Upon further investigations in the next step such as modulating the ratio of ZnO/CNO and analyzing real samples like blood serum and urine, it will be helpful for a better understanding of the mechanism behind the determination of glucose and optimization of sensor performance to a more stable direction leading to integration to POC devices or wearable sensors.

## 4. EXPERIMENTAL SECTION

**4.1. Chemicals.** Zinc nitrate hexahydrate [{Zn-$(NO_3)_2.6H_2O$}, ≥96%] was purchased from Merck, sodium hydroxide (NaOH, 97%) was purchased from Fisher Scientific, whereas d-(+)-glucose, L-ascorbic acid (AA, 99%), urea crystal (99%), citric acid (CA, 99%), glycerol (99%), polyvinylidene difluoride (PVDF), and *N*-methyl pyrrolidone (NMP) were purchased from Sigma-Aldrich Corporation. All the chemicals used were of analytical-grade quality. Ethanol, deionized (DI) water, and acetone were used as received without any purity alterations.



https://doi.org/10.1021/acsomega.2c04730
ACS Omega 2022, 7, 37748−37756

**4.2. Synthesis of ZnO Nanostructures.** Solution A of zinc nitrate hexahydrate [$Zn(NO_3)_2.6H_2O$] was prepared by adding 8.8 g of zinc nitrate in 160 mL of DI water under constant stirring at 90 °C. Simultaneously, solution B was prepared by dissolving 8 g of NaOH solution in 40 mL of DI water. Solution B (32 mL) was added dropwise to solution A, and the resultant solution turns to milky white. Finally, this solution is kept for stirring for another 2 h at 90 °C, and after the reaction, the solution was left overnight to settle down the precipitate. The next day, the precipitate was washed and centrifuged several times with DI water (at least five times) and placed in an oven at 90 °C for drying for 24 h. Annealing of the obtained ZnO powder was done at 500 °C for 2 h using a vertical furnace, and the heat rate was 5 °C per minute.[53] The morphology and purity were confirmed by XRD, SEM, and UV−visible spectra.

**4.3. Synthesis of CNOs.** To synthesize the CNOs, the previously reported method (flame pyrolysis method)[48] was used. The flaxseed oil was pyrolyzed in an earthen pot under steady air conditions. The soot was deposited on the clean upturned glass beaker. After that, annealing of the soot was done at 500 °C for 2 h in the air furnace to remove the amorphous carbon or some unburnt oil. The prepared CNOs are kept in an airtight container under dry conditions.

**4.4. Synthesis of the ZnO/CNO Composite.** Here, the ZnO/CNO composite was mixed in a 1:1 ratio, and for this purpose, CNOs (50 mg) were dissolved in 30 mL of DI water and kept for sonication for 1 h. After that, ZnO (50 mg) was added to the above solution and put on the magnetic stirrer at 500 rpm for 24 h. The next day, the resultant solution was filtered out using Whatman filter paper and kept for drying at room temperature. Upon complete drying, the composite was scratched out with the help of a spatula, then weighed, and collected in Eppendorf. The synthesized materials were characterized using UV−vis, XRD, FTIR, SEM, and TEM techniques.

**4.5. Characterizations.** The optical absorption spectra were observed using a UV−visible spectrophotometer (UV−vis, LAMBDA 750 PerkinElmer) in the 200−800 nm wavelength range. The morphology and particle size of all the samples were analyzed using field emission scanning electron microscopy [FESEM; Nova Nano FE-SEM 450 FEI] and high-resolution transmission electron microscopy [HRTEM; Tecnai G220 (FEI) S-TWIN]. The crystallization of nanostructures was observed through X-ray diffraction patterns recorded at room temperature by a PANalytical X'Pert Pro X-ray diffractometer applying a Cu K$\alpha$ radiation source at $\lambda$ = 1.5406 Å. The FTIR spectra were obtained using an FTIR spectrometer [PerkinElmer Spectrum version 10.4.00] in the range of 4000−400 $cm^{-1}$.

**4.6. Electrochemical Glucose Sensing in 0.1 M NaOH (Electrochemical Sensing Measurement) and Modification of Working Electrodes.** All the electrochemical sensing measurements were performed in a three-electrode setup using glassy carbon as a working electrode, Pt wire as a counter electrode, Ag/AgCl (in saturated KCl) as a reference electrode, and 0.1 M NaOH as an electrolyte.

The glassy carbon electrode was polished with 1.0, 0.3, and 0.05 $\mu$m of alumina powders to achieve a shiny mirror surface and after each polishing process rinsed with DI water. The active surface area of the glassy carbon electrode was around 0.071 $cm^2$ with a 3 mm diameter. For the preparation of the working electrode, a slurry is prepared by mixing the annealed ZnO (10 mg) and PVDF (1.11 mg) in a 9:1 ratio with the addition of 1−2 drops of NMP. Then, the slurry was coated on a glassy carbon electrode and dried overnight at room temperature. The active mass loading of the electrode was around 1.53 mg. For the preparation of the modified ZnO/CNO electrode and CNO electrode, the procedure was the same.

All the measurements were performed using an electrochemical workstation (CHI760E) at room temperature under constant stirring. CV measurements were done in the potential range of −1.6 to +1.6 V at a scan rate of 50 mV/sec. For amperometric measurement, the potential was fixed at 0.65 V, and the measurement was performed for 10 min.

## AUTHOR INFORMATION


### Corresponding Authors

**Kamlendra Awasthi** − *Department of Physics, Malaviya National Institute of Technology, Jaipur 302017, India;* orcid.org/0000-0002-4407-1914; Email: kawasthi.phy@mnit.ac.in

**Anjali Awasthi** − *Department of Zoology, University of Rajasthan, Jaipur 302004, India;* orcid.org/0000-0001-7209-8666; Email: anjkam.awasthi@gmail.com

### Authors

**Ankita Sharma** − *Department of Zoology, University of Rajasthan, Jaipur 302004, India*

**Ankush Agrawal** − *Department of Zoology, University of Rajasthan, Jaipur 302004, India;* orcid.org/0000-0002-0916-4058

**Gaurav Pandey** − *Department of Physics, Malaviya National Institute of Technology, Jaipur 302017, India*

**Sanjay Kumar** − *Department of Physics, Malaviya National Institute of Technology, Jaipur 302017, India*

Complete contact information is available at: https://pubs.acs.org/10.1021/acsomega.2c04730


### Notes

The authors declare no competing financial interest.

## ACKNOWLEDGMENTS

The authors would like to thank MRC MNIT Jaipur for its characterization facilities. The authors also acknowledge the support from Dr. Debasish Sarkar, MNIT Jaipur, for allowing electrochemical measurements. A.S. and A.A. acknowledge UGC (New Delhi) and CSIR (New Delhi), respectively, for financial support.

## REFERENCES

(1) Alsufyani, T.; Fadlallah, S. A. Detection of Glucose in the Growth Media of Ulva Lactuca Using a Ni-Cu/TiO2/Ti Self-Assembly Nanostructure Sensor under the Influence of Crude Oil. *Sens. Biosensing Res.* **2017**, *14*, 7−16.

(2) Farah, A. A.; Sukor, R.; Fatimah, A. B.; Jinap, S.*Application of Nanomaterials in the Development of Biosensors for Food Safety and Quality Control*; 2016; Vol. 23.

(3) *IDF Diabetes Atlas 10th Edition*. 2021

(4) Raymundo-Pereira, P. A.; Shimizu, F. M.; Coelho, D.; Piazzeta, M. H. O.; Gobbi, A. L.; Machado, S. A. S.; Oliveira, O. N. A Nanostructured Bifunctional Platform for Sensing of Glucose Biomarker in Artificial Saliva: Synergy in Hybrid Pt/Au Surfaces. *Biosens. Bioelectron.* **2016**, *86*, 369−376.

(5) Myndrul, V.; Coy, E.; Babayevska, N.; Zahorodna, V.; Balitskyi, V.; Baginskiy, I.; Gogotsi, O.; Bechelany, M.; Giardi, M. T.;



https://doi.org/10.1021/acsomega.2c04730
ACS Omega 2022, 7, 37748−37756

Iatsunskyi, I. MXene Nanoflakes Decorating ZnO Tetrapods for Enhanced Performance of Skin-Attachable Stretchable Enzymatic Electrochemical Glucose Sensor. *Biosens. Bioelectron.* **2022**, *207*, No. 114141.
(6) Zhao, Z. W.; Chen, X. J.; Tay, B. K.; Chen, J. S.; Han, Z. J.; Khor, K. A. A Novel Amperometric Biosensor Based on ZnO:Co Nanoclusters for Biosensing Glucose. *Biosens. Bioelectron.* **2007**, *23*, 135−139.
(7) Xu, R.; Jiang, Y.; Xia, L.; Zhang, T.; Xu, L.; Zhang, S.; Liu, D.; Song, H. A Sensitive Photoelectrochemical Biosensor for AFP Detection Based on ZnO Inverse Opal Electrodes with Signal Amplification of CdS-QDs. *Biosens. Bioelectron.* **2015**, *74*, 411−417.
(8) Özcan, L.; Şahin, Y.; Türk, H. Non-Enzymatic Glucose Biosensor Based on Overoxidized Polypyrrole Nanofiber Electrode Modified with Cobalt(II) Phthalocyanine Tetrasulfonate. *Biosens. Bioelectron.* **2008**, *24*, 512−517.
(9) Hwang, D.-W.; Lee, S.; Seo, M.; Chung, T. D. Recent Advances in Electrochemical Non-Enzymatic Glucose Sensors − A Review. *Anal. Chim. Acta* **2018**, 1−34.
(10) Adeel, M.; Rahman, M. M.; Caligiuri, I.; Canzonieri, V.; Rizzolio, F.; Daniele, S. Recent Advances of Electrochemical and Optical Enzyme-Free Glucose Sensors Operating at Physiological Conditions. *Biosens. Bioelectron.* **2020**, No. 112331.
(11) Romanholo, P. V. V.; Razzino, C. A.; Raymundo-Pereira, P. A.; Prado, T. M.; Machado, S. A. S.; Sgobbi, L. F. Biomimetic Electrochemical Sensors: New Horizons and Challenges in Biosensing Applications. *Biosens. Bioelectron.* **2021**, No. 113242.
(12) Tee, S. Y.; Teng, C. P.; Ye, E. Metal Nanostructures for Non-Enzymatic Glucose Sensing. *Mater. Sci. Eng., C* **2017**, *70*, 1018−1030.
(13) Golsanamlou, Z.; Mahmoudpour, M.; Soleymani, J.; Jouyban, A. Applications of Advanced Materials for Non-Enzymatic Glucose Monitoring: From Invasive to the Wearable Device. *Crit. Rev. Anal. Chem.* **2021**, 1.
(14) Kianfar, E.*Catalytic Properties of Nanomaterials and Factors Affecting It*; MedDocs Publishers, 2020; Vol. *5*.
(15) Sharma, A.; Agrawal, A.; Awasthi, K. K.; Awasthi, K.; Awasthi, A. Biosensors for Diagnosis of Urinary Tract Infections: Advances and Future Challenges. *Mater. Lett.: X* **2021**, *10*, No. 100077.
(16) Solanki, P. R.; Kaushik, A.; Agrawal, V. V.; Malhotra, B. D.Nanostructured Metal Oxide-Based Biosensors. *NPG Asia Mater.*2011, pp. 17−24, DOI: 10.1038/asiamat.2010.137.
(17) Zhu, H.; Li, L.; Zhou, W.; Shao, Z.; Chen, X. Advances in Non-Enzymatic Glucose Sensors Based on Metal Oxides. *J. Mater. Chem. B* **2016**, 7333−7349.
(18) Vinoth, V.; Subramaniyam, G.; Anandan, S.; Valdés, H.; Manidurai, P. Non-Enzymatic Glucose Sensor and Photocurrent Performance of Zinc Oxide Quantum Dots Supported Multi-Walled Carbon Nanotubes. *Mater. Sci. Eng.: B* **2021**, *265*, No. 115036.
(19) Haghparas, Z.; Kordrostami, Z.; Sorouri, M.; Rajabzadeh, M.; Khalifeh, R. Fabrication of Non-Enzymatic Electrochemical Glucose Sensor Based on Nano-Copper Oxide Micro Hollow-Spheres. *Biotechnol. Bioprocess Eng.* **2020**, *25*, 528−535.
(20) Sun, D.; Lu, J.; Wang, X.; Zhang, Y.; Chen, Z. Voltammetric Aptamer Based Detection of HepG2 Tumor Cells by Using an Indium Tin Oxide Electrode Array and Multifunctional Nanoprobes. *Microchim. Acta* **2017**, *184*, 3487−3496.
(21) Kumar Jangir, L.; Kumari, Y.; Kumar, A.; Kumar, M.; Awasthi, K. Investigation of Luminescence and Structural Properties of ZnO Nanoparticles, Synthesized with Different Precursors. *Mater. Chem. Front.* **2017**, *1*, 1413−1421.
(22) Sharma, A.; Agrawal, A.; Kumar, S.; Awasthi, K. K.; Awasthi, K.; Awasthi, A.Zinc Oxide Nanostructures-Based Biosensors. In *Nanostructured Zinc Oxide: Synthesis, Properties and Applications*; Elsevier: 2021, DOI: 10.1016/B978-0-12-818900-9.00002-4.
(23) Shetti, N. P.; Bukkitgar, S. D.; Reddy, K. R.; Reddy, C. V.; Aminabhavi, T. M. ZnO-Based Nanostructured Electrodes for Electrochemical Sensors and Biosensors in Biomedical Applications. *Biosens. Bioelectron.* **2019**, No. 111417.
(24) Qian, J.; Wang, Y.; Pan, J.; Chen, Z.; Wang, C.; Chen, J.; Wu, Z.; Yangyue. Non-Enzymatic Glucose Sensor Based on ZnO−CeO2 Whiskers. *Mater. Chem. Phys.* **2020**, *239*, No. 122051.
(25) Mai, H. H.; Tran, D. H.; Janssens, E. Non-Enzymatic Fluorescent Glucose Sensor Using Vertically Aligned ZnO Nanotubes Grown by a One-Step, Seedless Hydrothermal Method. *Microchim. Acta* **2019**, *186*, 1.
(26) Damberga, D.; Fedorenko, V.; Grundšteins, K.; Altundal, Ş.; Šutka, A.; Ramanavičius, A.; Coy, E.; Mrówczyński, R.; Iatsunskyi, I.; Viter, R. Influence of Pda Coating on the Structural, Optical and Surface Properties of Zno Nanostructures. *Nanomaterials* **2020**, *10*, 2438.
(27) Agarwal, S.; Rai, P.; Gatell, E. N.; Llobet, E.; Güell, F.; Kumar, M.; Awasthi, K. Gas Sensing Properties of ZnO Nanostructures (Flowers/Rods)Synthesized by Hydrothermal Method. *Sens. Actuators, B* **2019**, *292*, 24−31.
(28) Agarwal, S.; Kumar, S.; Agrawal, H.; Moinuddin, M. G.; Kumar, M.; Sharma, S. K.; Awasthi, K. An Efficient Hydrogen Gas Sensor Based on Hierarchical Ag/ZnO Hollow Microstructures. *Sens. Actuators, B* **2021**, *346*, No. 130510.
(29) Tarlani, A.; Fallah, M.; Lotfi, B.; Khazraei, A.; Golsanamlou, S.; Muzart, J.; Mirza-Aghayan, M. New ZnO Nanostructures as Non-Enzymatic Glucose Biosensors. *Biosens. Bioelectron.* **2015**, *67*, 601−607.
(30) Raza, W.; Ahmad, K. A Highly Selective Fe@ZnO Modified Disposable Screen Printed Electrode Based Non-Enzymatic Glucose Sensor (SPE/Fe@ZnO). *Mater. Lett.* **2018**, *212*, 231−234.
(31) Mahmoud, A.; Echabaane, M.; Omri, K.; el Mir, L.; Chaabane, R. B. Development of an Impedimetric Non Enzymatic Sensor Based on ZnO and Cu Doped ZnO Nanoparticles for the Detection of Glucose. *J. Alloys Compd.* **2019**, *786*, 960−968.
(32) Martoni, L. V. L.; Gomes, N. O.; Prado, T. M.; Calegaro, M. L.; Oliveira, O. N., Jr.; Machado, S. A. S.; Raymundo-Pereira, P. A. Carbon Spherical Shells in a Flexible Photoelectrochemical Sensor to Determine Hydroquinone in Tap Water. *J. Environ. Chem. Eng.* **2022**, *10*, No. 107556.
(33) Raymundo-Pereira, P. A.; Gomes, N. O.; Machado, S. A. S.; Oliveira, O. N., Jr. Wearable Glove-Embedded Sensors for Therapeutic Drug Monitoring in Sweat for Personalized Medicine. *Chem. Eng. J.* **2022**, *435*, No. 135047.
(34) Baccarin, M.; Ciciliati, M. A.; Oliveira, O. N., Jr.; Cavalheiro, E. T. G.; Raymundo-Pereira, P. A. Pen Sensor Made with Silver Nanoparticles Decorating Graphite-Polyurethane Electrodes to Detect Bisphenol-A in Tap and River Water Samples. *Mater. Sci. Eng., C* **2020**, *114*, No. 110989.
(35) Kour, R.; Arya, S.; Young, S.-J.; Gupta, V.; Bandhoria, P.; Khosla, A. Review—Recent Advances in Carbon Nanomaterials as Electrochemical Biosensors. *J. Electrochem. Soc.* **2020**, *167*, No. 037555.
(36) Plonska-Brzezinska, M. E. Carbon Nano-Onions: A Review of Recent Progress in Synthesis and Applications. *ChemNanoMat* **2019**, 568−580.
(37) Sok, V.; Fragoso, A. Amperometric Biosensor for Glyphosate Based on the Inhibition of Tyrosinase Conjugated to Carbon Nano-Onions in a Chitosan Matrix on a Screen-Printed Electrode. *Microchim. Acta* **2019**, *186*, 1.
(38) Sohouli, E.; Ghalkhani, M.; Zargar, T.; Joseph, Y.; Rahimi-Nasrabadi, M.; Ahmadi, F.; Plonska-Brzezinska, M. E.; Ehrlich, H. A New Electrochemical Aptasensor Based on Gold/Nitrogen-Doped Carbon Nano-Onions for the Detection of Staphylococcus Aureus. *Electrochim. Acta* **2022**, *403*, No. 139633.
(39) Mohapatra, J.; Ananthoju, B.; Nair, V.; Mitra, A.; Bahadur, D.; Medhekar, N. v.; Aslam, M. Enzymatic and Non-Enzymatic Electrochemical Glucose Sensor Based on Carbon Nano-Onions. *Appl. Surf. Sci.* **2018**, *442*, 332−341.
(40) Tripathi, K. M.; Bhati, A.; Singh, A.; Gupta, N. R.; Verma, S.; Sarkar, S.; Sonkar, S. K. From the Traditional Way of Pyrolysis to Tunable Photoluminescent Water Soluble Carbon Nano-Onions for


https://doi.org/10.1021/acsomega.2c04730
*ACS Omega* 2022, 7, 37748−37756

Cell Imaging and Selective Sensing of Glucose. *RSC Adv.* **2016**, *6*, 37319−37329.
(41) Vélez, C. A.; Soto-Pérez, J. J.; Corchado-García, J.; Larios, E.; Fulvio, P. F.; Echegoyen, L.; Cabrera, C. R. Glucose Oxidation Reaction at Palladium-Carbon Nano-Onions in Alkaline Media. *J. Solid State Chem.* **2021**, 207.
(42) Cai, B.; Zhou, Y.; Zhao, M.; Cai, H.; Ye, Z.; Wang, L.; Huang, J. Synthesis of ZnO−CuO Porous Core−Shell Spheres and Their Application for Non-Enzymatic Glucose Sensor. *Appl. Phys. A: Mater. Sci. Process.* **2015**, *118*, 989−996.
(43) Singh, K.; Umar, A.; Kumar, A.; Chaudhary, G. R.; Singh, S.; Mehta, S. K. Non-Enzymatic Glucose Sensor Based on Well-Crystallized ZnO Nanoparticles. *Sci. Adv. Mater.* **2012**, *4*, 994−1000.
(44) Ahmad, R.; Tripathy, N.; Ahn, M. S.; Bhat, K. S.; Mahmoudi, T.; Wang, Y.; Yoo, J. Y.; Kwon, D. W.; Yang, H. Y.; Hahn, Y. B. Highly Efficient Non-Enzymatic Glucose Sensor Based on CuO Modified Vertically-Grown ZnO Nanorods on Electrode. *Sci. Rep.* **2017**, *7*, 1.
(45) Khan, S.; Rasheed, M. A.; Waheed, A.; Shah, A.; Mahmood, A.; Ali, T.; Nisar, A.; Ahmad, M.; Karim, S.; Ali, G. The Role of Electrodeposition Current Density in the Synthesis and Non-Enzymatic Glucose Sensing of Oxidized Zinc-Tin Hybrid Nanostructures. *Mater. Sci. Semicond. Process.* **2020**, *109*, No. 104953.
(46) Afreen, S.; Muthoosamy, K.; Manickam, S.; Hashim, U. Functionalized Fullerene (C60) as a Potential Nanomediator in the Fabrication of Highly Sensitive Biosensors. *Biosens. Bioelectron.* **2015**, 354−364.
(47) Agarwal, S.; Jangir, L. K.; Rathore, K. S.; Kumar, M.; Awasthi, K. Morphology-Dependent Structural and Optical Properties of ZnO Nanostructures. *Appl. Phys. A: Mater. Sci. Process.* **2019**, *125*, 1.
(48) Park, S. J.; Das, G. S.; Schütt, F.; Adelung, R.; Mishra, Y. K.; Tripathi, K. M.; Kim, T. Y. Visible-Light Photocatalysis by Carbon-Nano-Onion-Functionalized ZnO Tetrapods: Degradation of 2,4-Dinitrophenol and a Plant-Model-Based Ecological Assessment. *NPG Asia Mater.* **2019**, *11*, 1.
(49) Mohajeri, S.; Dolati, A.; Yazdanbakhsh, K. Synthesis and Characterization of a Novel Non-Enzymatic Glucose Biosensor Based on Polyaniline/Zinc Oxide/Multi-Walled Carbon Nanotube Ternary Nanocomposite. *J. Electrochem. Sci. Eng.* **2019**, *9*, 207−222.
(50) Chen, H. C.; Su, W. R.; Yeh, Y. C. Functional Channel of SWCNTs/Cu2O/ZnO NRs/Graphene Hybrid Electrodes for Highly Sensitive Nonenzymatic Glucose Sensors. *ACS Appl. Mater. Interfaces* **2020**, *12*, 32905−32914.
(51) Manna, A. K.; Guha, P.; Solanki, V. J.; Srivastava, S. K.; Varma, S. Non-Enzymatic Glucose Sensing with Hybrid Nanostructured Cu2O-ZnO Prepared by Single-Step Coelectrodeposition Technique. *J. Solid State Electrochem.* **2020**, *24*, 1647−1658.
(52) Liu, M.; Liu, R.; Chen, W. Graphene Wrapped Cu2O Nanocubes: Non-Enzymatic Electrochemical Sensors for the Detection of Glucose and Hydrogen Peroxide with Enhanced Stability. *Biosens. Bioelectron.* **2013**, *45*, 206−212.
(53) Kumar, S.; Awasthi, K.; Mishra, Y. K.Synthesis of ZnO Nanostructures. In *Nanostructured Zinc Oxide: Synthesis, Properties and Applications*; Elsevier: 2021, DOI: 10.1016/B978-0-12-818900-9.00016-4.


https://doi.org/10.1021/acsomega.2c04730
*ACS Omega* 2022, 7, 37748−37756